Splashing physics of springboard diving

Heck, A. ; van Baarsen, S.; Heinzel, J.W.; Mooldijk, A.; van Veen, N.

DOI
10.1088/1361-6552/ad9fcb

Publication date
2025

Document Version
Final published version

Published in
Physics Education

OPEN ACCESS

PAPER

Phys. Educ. **60** (2025) 025004 (17pp)

iopscience.org/ped

Splashing physics of springboard diving

André Heck[1,*], **Sebas van Baarsen**[2], **Jan Wilko Heinzel**[2], **Ad Mooldijk**[3] **and Norbert van Veen**[3]

[1] Korteweg-de Vries Institute for Mathematics, University of Amsterdam, Amsterdam, The Netherlands
[2] Indoor Cliff Diving, Amsterdam, The Netherlands
[3] CMA-Science, Amsterdam, The Netherlands

E-mail: a.j.p.heck@uva.nl

Abstract

Understanding rotational physics is often difficult due to abstract concepts like torque, angular momentum, and moments of inertia, along with the required knowledge of trigonometry and calculus. This paper presents how springboard diving and gymnastics offer real-world contexts for students to explore these topics, focusing on non-twisting somersaults in springboard diving. Video analysis, body modelling, and motion analysis are suggested as student activities to deepen their understanding of biomechanics and rotational physics, specifically in estimating body segment inertia parameters and analysing somersaults.

Keywords: rotational kinetics, biomechanics, video analysis, anthropometric modelling of the human body, estimation of moments of inertia and angular momentum

Supplementary material for this article is available online

1. Introduction

Gymnastics, trampolining, and springboard diving rely heavily on physics to create complex movements, making these sports ideal for studying rotational kinetics. While traditional exercises focus on basic calculations of an angular velocity change due to a change in moment of inertia, rich contexts for studying rotational physics, such as the giant circle on the high bar [1, 2], the Jäger salto [3], and a toppling dive from a standing position on a springboard [4], involve activities where upper-secondary students and beyond really use physics and mathematics concepts to understand human movements. This paper explores somersaults in diving from a 3m springboard, where body rotation occurs predominantly in the air and postural changes determine the amount of rotation. We present student activities for investigating diving using simple measurement tools, video

* Author to whom any correspondence should be addressed.

analysis, and body models. We restrict the study to non-twisting somersaults, carried out by two elite cliff divers. We use the COACH environment [5, 6] for video analysis and data analysis.

2. Bird's eye view of springboard diving and biomechanical research

This section provides a brief overview of springboard diving and related biomechanical research. We

1. describe the different phases of a dive;
2. explain the naming conventions for competitive dives;
3. discuss the orientation of the athlete's body during a dive;
4. outline the biomechanical principles that help understand the athlete's movements during the flight phase.

2.1. Phases of a springboard dive

A springboard dive consists of five main phases: starting position, approach, take-off, flight, and water entry. In competitive diving, the primary goals are to generate sufficient angular momentum to execute an announced number of twists and somersaults, maximise air time, and control the distance from the board to achieve the best score. These objectives are largely determined at the end of the take-off. Once airborne, the athlete can only adjust the somersault speed by changing body shape. Angular momentum needed to initiate rotation is generated through hip flexion before leaving the board, as it remains constant once airborne. This is a conceptual understanding of rotational dynamics that students need to come to grips with before they can explore somersaults in depth.

2.2. Dive number

A dive number is an alphanumeric code that specifies the dive being performed. For example, 107 C represents a forward (1) somersault (0) with three-and-a-half rotations (7) in a tucked posture (C). The code always starts with three or four digits followed by a letter. The third digit shows the number of half somersaults and the letter denotes the main body posture during flight: A for layout, B for piked, C for tucked, D for free posture. The layout, piked, and tucked postures are defined by the angles of the hip and knee joints (see [7]).

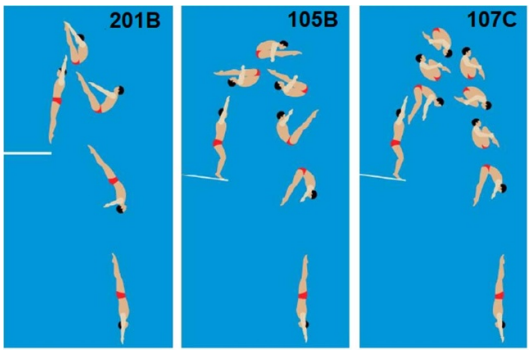

Figure 1. Artist impressions of diving figures (after [8]). In the 201B and 105B dives, the athlete changes posture from layout to pike, and back to layout. In the 107 C dive, the athlete changes posture from layout to tuck, and back to layout.

Figure 1 shows artist impressions of diving figures discussed in this paper, illustrating differences between backward and forward diving, and between a layout, piked and tucked posture during a dive.

Figure 2 overlays video images of a 107C and a 103B dive (forward $1\frac{1}{2}$ somersault in a piked posture), showing the athlete leaning forward at take-off to generate rotation. Since angular momentum is conserved, the diver cannot stop mid-air, so underwater movements create the illusion of a vertical entry.

2.3. Body orientation angle

A non-twisting somersault involves body rotation about a horizontal axis parallel to the ground and perpendicular to the direction of travel, aligning with the body's transverse axis. This rotation is described by a moving non-rotating 3D reference frame centred at the athlete's centre of gravity (CG), with the positive z-axis vertically upward, the y-axis horizontal parallel to the transverse axis

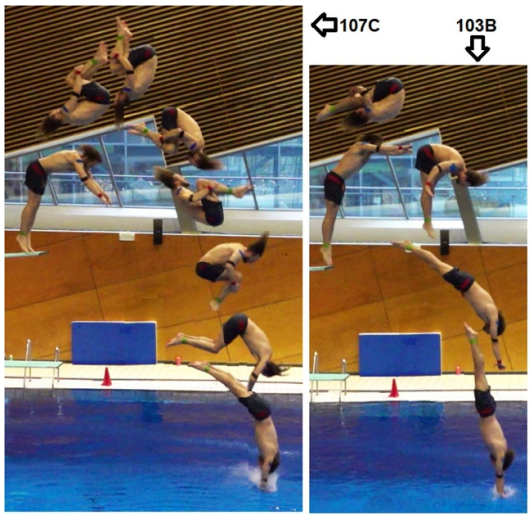

Figure 2. Overlays of images of postures during a video recorded dive with dive number 107C (left) and 103B (right).

Figure 3. A series of stills from a video recording of a 201B dive, from layout to layout posture via an intermediate piked posture. The time lapse between consecutive stills is 2/15 s.

and directed from left to right, and the x-axis following the direction of travel for forward and backward somersaults.

When the athlete maintains a fixed posture during flight, the body can be treated as a single unit, and a specific point or body segment can be used to describe the rotation. In section 3 we use this method to describe the rotation of a diver in a tucked posture during a 107C dive. However, posture changes complicate this, as seen in a 201B dive (figure 3) where the torso and lower extremities rotate in opposite directions, making it difficult to describe clockwise whole-body rotation at low speed.

Yeadon [9] proposed using the orientation of the line from the midpoint of the knee to the midpoint of the shoulder, as it is less sensitive to hip angle changes than using a single body segment. The angle between this line and the

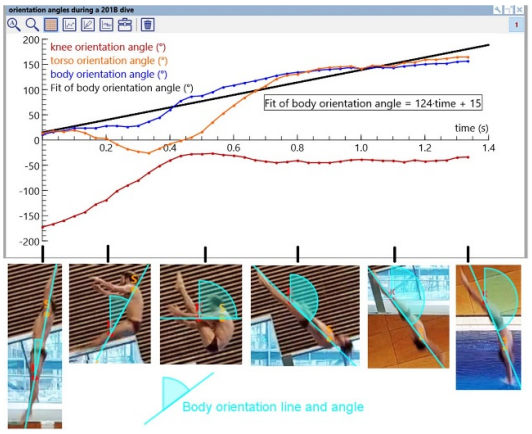

Figure 4. Graphs of three orientation angles in a 201B dive.

vertical axis is called the body orientation angle. Figure 4 shows this angle over time for a 201B dive (blue graph), with a nearly constant rotation at 124°/s (the slope of the linear fit in black). The other graphs, based on the orientation angles of lines through the hip and torso (orange graph) and the lower extremities (red graph) illustrate that these angles are less suitable for describing whole-body rotation. As the diver straightens before water entry, the torso and body orientation angles converge, though not perfectly straight as in the artistic depiction in figure 1. Video stills below the diagram show the body orientation line and angle at several moments: take-off ($t = 0$), mid-flight ($t = 0.2$, 0.5, 0.8, 1.1), and water entry ($t = 1.33$ s).

We propose using the orientation of the line from the CG of the lower extremity to the torso's CG, avoiding knee position measurements in piked dives. We call the angle between the vertical axis and this line the somersault angle. Discussing body orientation during somersaults in class confronts students with the fact that definitions in physics are often ambiguous when applied to real-world contexts. In diving, dive height and flight time can also be interpreted in many ways. Once clear definitions are established, students can explore how these quantities and body segment angles change during a dive, and compare data across differing diving figures and athletes, much like sports scientists do in research practice.

2.4. Biomechanical principles for understanding somersaults

Understanding somersaults requires grasping key principles of rotational dynamics, including angular velocity and acceleration, torque, angular momentum, and moment of inertia. These concepts are challenging for students, who often hold alternative conceptions [10, 11]. Somersaults combine planar motion (about a point mass) and the rotation of a non-rigid body with rigid segments. Learning typically begins with (a system of) point-like objects and advances to a system of rigid bodies that can change positions relative to each other. Video analysis activities [2, 12–14] and lab experiments with sensors [15] are recommended to help students grasp the physics of rotational motion. Focusing on pure somersaults, where rotation occurs about an axis perpendicular to the motion plane, simplifies the analysis to linear and angular kinetics.

2.4.1. Centre of gravity. Students must understand the centre of gravity (CG) as the point where the body's mass is concentrated and through which gravity acts. It may lie outside the body depending on the arrangement and relative masses of body segments. To determine it, anthropometric models like a five-segment model (two upper extremities, two lower extremities, and the head-neck-torso; see figure 5) and (a) more complex nine-segment model (Woolley's model [16], discussed in section 4) are used. The CG for the whole body is calculated by combining the mass and CG for each segment, with values estimated from biomechanics textbooks [17–19], which also provide detailed information and examples about these calculations. Figure 5 illustrates the calculation for a 5-segment human body model.

2.4.2. Moment of inertia and angular momentum. Another opportunity for students to expand their knowledge is thinking about how to approximate the angle of rotation for describing somersault dynamics. In this paper we use the body orientation angle for this purpose. Angular velocity ω is the rate of change of this angle. The angular momentum L, or more precisely its magnitude, is expressed as $L = I \cdot \omega$, where I is the moment of

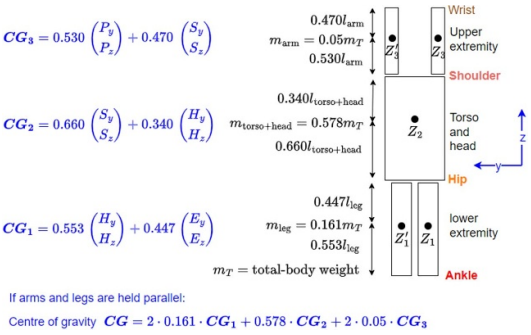

Figure 5. Sample calculation of the location of the centre of gravity for a five-segment human body model.

inertia of the human body about the axis of rotation. Both ω and I change during a somersault due to postural changes, but their product remains constant. I is calculated by summing the moments of inertia for all segments, estimated using geometrical modelling and the parallel axis theorem (see section 4).

A more precise method, which does not rely on an ambiguous angle of rotation or treatment of the body as a single non-rigid object, calculates the angular momentum L_s of each segment s using a local and remote term [17, 18]:

$$L_s = I_s \cdot \omega_s + m_S \cdot {d_s}^2 \cdot \omega_g .$$

In the local term, I_s and ω_s are the moment of inertia and the angular velocity with respect to a transverse axis through the segment's CG, respectively. In the remote term, m_S is the segment mass, d_s is the distance between the segment's CG and the body's CG, and ω_g is the angular velocity of the segment's centre of about the transverse axis through CG. If ω_s and ω_g are equal (denoted by ω), this simplifies to $L_s = \left(I_s + m_S \cdot {d_s}^2\right) \cdot \omega$. According to the parallel axis theorem, this can be written as $L_s = I(s) \cdot \omega$, where $I(s)$ is the moment of inertia of the segment s about the axis of rotation through the body's CG. So we are back to the formula where ω is the rate of change of the body orientation angle. But one must keep in mind that it is valid only when the athlete maintains a fixed posture in an airborne somersault. In general, the remote term is calculated using the cross product of the position vector $\overrightarrow{r_s}$ and the velocity vector

$\vec{v_s}$ of the segment's CG. The total body angular momentum L can then be computed as:

$$L = \sum_s I_s \cdot \omega_s + \sum_s m_s \cdot \left[\vec{r_s} \times \vec{v_s} \right]_3.$$

This formula is advantageous because the required vectors in the second sum can be determined using video analysis and data analysis tools, like the ones available in COACH [5, 6]. The moment of inertia I_s of segment s is usually expressed as

$$I_s = m_s \cdot {k_s}^2 = m_s \cdot (\rho_s \cdot l_s)^2$$

where k_s is the radius of gyration, which is often expressed as the proportion ρ_s of the segment's length l_s. Estimates of radii of gyrations of human body segments are available in many biomechanics textbooks [17–19]; we use table 4.1 in [17].

3. Motion analysis of a 107C dive

Using video analysis, the forward $3\frac{1}{2}$ somersault in a tucked posture from a 3-m springboard is analysed. Figure 6 highlights the athlete exiting the tuck and preparing for water entry. Yellow points mark the head's position, while orange dots trace the centre of gravity (CG), estimated from the head's motion while the athlete is in a tucked posture.

The analysis assumes that the motion is decomposed into a parabolic path of the CG under gravity and a sinusoidal trajectory to describe the body rotation during the tuck. The computational engine for this analysis is the least squares regression method of peeling-off functions [20]. The lower-left window in figure 6 displays the scatter plot of the vertical position with a quadratic regression curve. The lower-right diagram shows the result of sinusoidal regression of the residual. The sum of the quadratic and sinusoidal fits accurately describes the vertical position diver's head, as shown by the corresponding curve in the upper-right diagram.

A similar analysis for the horizontal motion of the head reveals a linear trend function. Both analyses yield an angular velocity of 898°/s (≈ $2\frac{1}{2}$ rotations per second). The linear and quadratic trend functions of the head's position can serve as

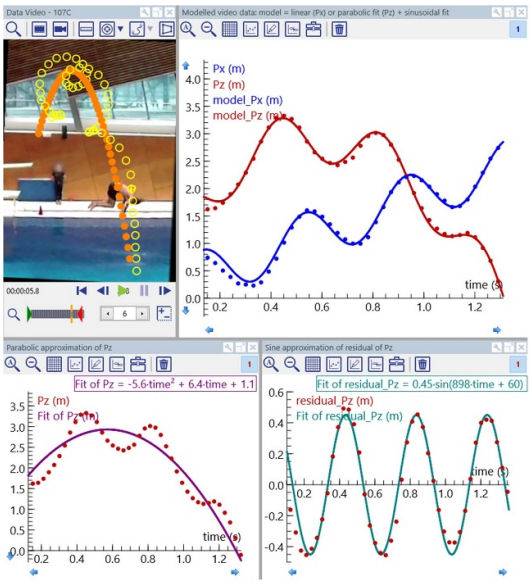

Figure 6. Video analysis of a 107C dive as compound motion. The lower windows show a parabolic fit of the vertical position of the athlete's head and a sinusoidal fit of its residual. The sum of these fits model the vertical position of the head, the graph of which is shown in the upper-right window, together with the model curve for the horizontal position of the head.

coordinate functions of the CG and displayed as overlay in the video clip, suggesting that it is in a tucked posture near the hip.

This observation motivates the exploration of the dive via a different method. Students may employ a moving coordinate system centred at the athlete's hip and measure the shoulder's position in polar coordinates. In essence, they use the hip-to-shoulder segment as the line of body orientation and determine the somersault angle. In figure 7, this method produces a scatter plot of the somersault angle (upper-right window). It is augmented with a linear fit, estimating the angular velocity at 907°/s, slightly higher than the first method's result.

The athlete's angular velocity during the somersault can be numerically computed as the derivative of the somersault angle. Students will observe that the angular velocity remains constant in the tucked posture and decreases before water entry. Figure 7's lower window, calculated using a spline-smoothing algorithm [21] and with the horizontal line fitted to the tucked posture

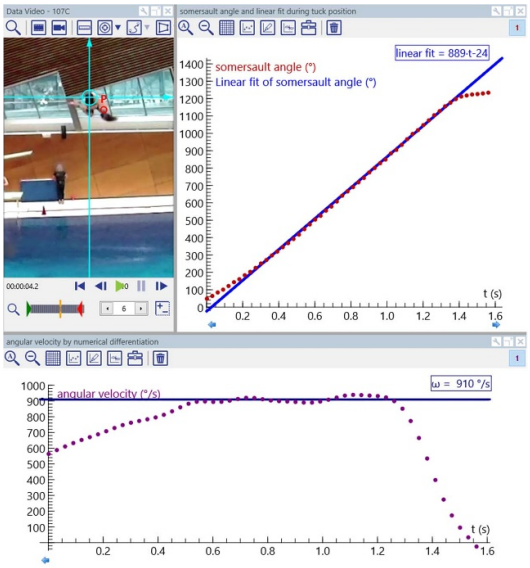

Figure 7. Video analysis of the somersault angle in a 107C dive, using the hip-shoulder segment as line of orientation.

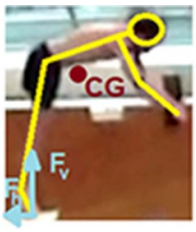

Figure 8. A stick model of the athlete at take-off, the position of the centre of gravity (CG), and the horizontal and vertical forces ($\overrightarrow{F_h}$ and $\overrightarrow{F_v}$) providing the torques to initiate forward.

period, confirms an angular velocity consistent with previous findings. The graph in the lower window of figure 7, connected with events in the video clip, indicate that changes in posture affect angular velocity.

For dives involving significant rotation, a net torque is needed to initiate rotation, which is generated during take-off (Frohlich [22] and others [23, 24] showed that limited rotation can occur without torque). Figure 8 shows the horizontal and vertical forces acting on a stick model of the athlete at the moment of leaving the springboard, providing the torques needed for a dive. An estimated CG is also shown.

Figure 8 does not capture the moment near the end of take-off, where the athlete bends the hips and throws the arms forward rapidly, generating angular momentum. If the body were free in space, the lower part would rotate in the opposite direction due to angular momentum conservation. However, as the athlete's feet are still in contact with the springboard, the board exerts a horizontal force on the athlete that resists this opposite direction. This horizontal and vertical reaction forces ($\overrightarrow{F_h}$ and $\overrightarrow{F_v}$) of the springboard when the athlete is leaning forward, with the CG not passing through the line of reaction force, provide the necessary torque to initiate the somersault. We believe that this qualitive analysis, described by Knudson [25] as 'systematic observation and introspective judgment of the quality of human movement for the purpose of providing the most appropriate intervention to improve performance,' is as important as quantitative analysis for understanding somersaults. Qualitative analysis helps students realise that qualitative biomechanical concepts are essential for understanding body movements. Quantitative analysis can substantiate or question qualitative outcomes, or provide more details, but it does not solely enhance conceptual understanding of mechanical laws. In section 5, we carry out a video analysis of a 105B dive (forward $2\frac{1}{2}$ somersault in a piked posture) to estimate kinematic variables and verify numerically the law of conservation of angular momentum.

4. Anthropometric modelling of the human body

Common assumptions in designing mathematical models of the human body include:

- The body is represented by rigid segments of simple geometric shapes and uniform density, approximating each body part's size, mass, and centre of mass;
- Regression equations for segment weights from research [26, 27] can be used in a biomechanical study;
- Limbs move about fixed pivot points, such as neck, shoulder, elbow, wrist, pelvis, knee, and ankle joints.

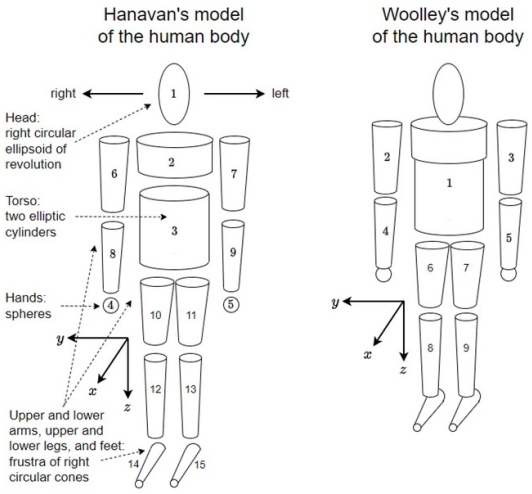

Figure 9. Hanavan's model of the human body and Woolley's simplification (after [16]).

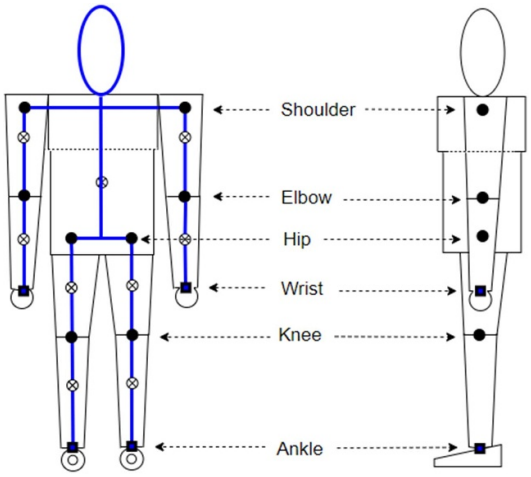

Figure 10. Front and side view of Woolley's model (not drawn to scale) with marked segment joints (closed circles) and local centres of gravity (open circles with a cross), and the wrists and ankles as distal points (closed squares) of the forearms and lower legs, respectively.

Hanavan [28] designed a 15-segment model (figure 9, left) requiring 25 anthropometric measurements to calculate properties of the model. Woolley [16] simplified it to a nine-segment model (figure 9, right) by combining the head, neck and torso into one segment, each lower arm with the hands, and each lower leg with the foot. We indicate the orientation of the coordinate system used to estimate inertial properties of segments on the basis of the geometrical shapes involved.

4.1. Mass distribution

Total body mass is distributed across segments using regression equations, with Barter's equations [26] being a common choice due to their simplicity compared to the method of Clauser *et al* [27], which requires body fat measurements. Following Woolley's approach, the mass input is adjusted so that the sum of the regression equations match the individual's body mass:

1. mass of head, neck, trunk $= HNT = 0.47m'_T +$ 5.44 kg
2. mass of both upper arms $= BUA = 0.08m'_T -$ 1.32 kg
3. mass of both forearms $= BFO = 0.04m'_T -$ 0.23 kg
4. mass of both hands $= BH = 0.01m'_T +$ 0.32 kg
5. mass of both upper legs $= BUL = 0.18m'_T +$ 1.45 kg
6. mass of both lower legs $= BLL = 0.11m'_T -$ 0.86 kg
7. mass of both feet $= BF = 0.02m'_T +$ 0.68 kg

where

$$m'_T = \frac{m_T - 5.48}{0.91}.$$

The corrected total mass of the modelled man m'_T distributes the total body mass m_T proportionately to the segment masses. The estimated segment weights are used in calculations.

4.2. Segments' centres of mass and moments of inertia

For computations of the centres of mass and moments of inertia for the athlete's body segments and the total body, we use the stick model of Woolley's model of the human body [16] shown in figure 10. This model simplifies a body into nine segments, with joints as endpoints, using geometric shapes:

- head (included in segment 1) as right circular ellipsoid;

- torso (included in segment 1 as right elliptic cylinder;
- hands (included in segments 4 and 5) as spheres.
- Upper arms (segments 2 and 3), lower arms (segments 4 and 5), upper legs (segments 6 and 7), lower legs (segments 8 and 9), and the feet (included in segments 8 and 9) as frustra of right circular cones.

Assuming uniform density, the local CG and the moment of inertia for each shape can be calculated. We do not expect that students derive formulas for computing moments of inertia about principle axes for the geometrical shapes used. Neither do we expect that they use the parallel axis theorem to compute moments of inertia of combined segments. They can simply look up formulas, based on twenty-five anthropometric dimensions, in the supplementary file *Anthropometric model of man*. The supplementary *JupyterLab notebook for Python* [29] contains the programming code for the computations.

4.3. Results of computations for two athletes

This section presents the estimated segmental centres of gravities and the moments of inertia about principal axes for the two athletes in this study, compared with literature results. The supplementary *Long write-up* file contains details.

The estimated centres of gravity, as percentages of segment length (from proximal to distal) for both athletes, match values from Miller and Morrison's summary of 30 male athletes [30]. Figure 11 visually represents the segmental centres of gravity for Athlete 1, along with the variables used in our computer programs for anthropometric computations. Such a visual aid is particularly useful for students. Despite using basic tools for the 25 anthropometric measurements, the results for Athlete 2 match literature values. But athlete 1's results show differences: The torso's CG is further from the proximal endpoint, and the thigh's is closer. This highlights individual variations in body composition.

Differences are more pronounced in the segmental *yy*-components of the moment of inertia

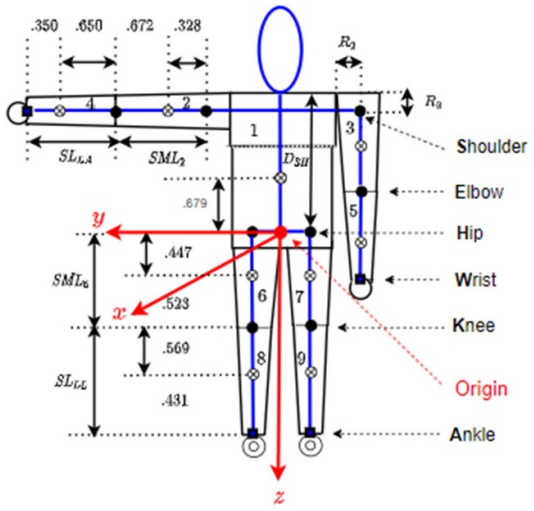

Figure 11. Body segment centres of gravity for Athlete 1 in Woolley's model of the human body.

listed in table 1, with Athlete 1 having a significantly smaller upper torso inertia compared to Athlete 2, though other segment differences are minor and match vales reported by Miller and Morrison [30].

Estimated centres of gravity and moments of inertia (*yy*-components), and segment lengths enable the calculation of radii of gyration, shown in table 2 alongside Dempster's values [31]. These align with data from Miller and Morrison [30]. However, Athlete 1's smaller radii of gyration, particularly in the upper torso, suggest a potential advantage in rotating this body part.

To explore this a bit further we compute moments of inertia of the human body about the transverse axis through the CG in five postures: (a) layout with hands stretched, downwards, (b) sideways, and (c) overhead, (d) pike, and (e) tuck (figure 12). The estimated values are listed in table 3.

The estimated moments of inertia (in $\mathrm{kg \cdot m^2}$) for the standing and tucked posture in table 3 are consistent with Whittset's findings [32]: 11.3 vs 12.3 and 3.4 vs 4.7, respectively. Athlete 2's inertia properties closely resemble those of the 'average athlete' from Miller and Morrison [301]. In contrast, Athlete 1 exhibits smaller moments of inertia across the five postures, suggesting a natural advantage for faster rotation with the same angular momentum generated at take-off.

Table 1. Estimated *yy*-components of the moments of inertia through the local segments' centres of gravity ($kg \cdot m^2$).

			Miller & Morrison	
Body part	Athlete 1	Athlete 2	Mean	Std.Dev
Head	0.0472	0.0471	0.0419	0.0104
Upper torso	0.0572	0.0926	0.1055	0.0366
Lower torso	0.4246	0.4512	0.4381	0.1453
Hand	0.0005	0.0005	0.0005	0.0001
Upper arm	0.0266	0.0360	0.0297	0.0109
Forearm	0.0057	0.0068	0.0098	0.0033
Thigh	0.0952	0.0967	0.1024	0.0301
Lower leg	0.0517	0.0752	0.0684	0.0246
Foot	0.0063	0.0079	0.0075	0.0018

Table 2. Estimated radii of gyration (as proportion of segment length) of body segments about axes parallel to the transverse axis through the segments' centres of gravity.

Body part	Athlete 1	Athlete 2	Miller & Morrison	Dempster
Upper torso	0.057	0.093	0.106	
Lower torso	0.425	0.451	0.438	
Entire torso	0.371	0.410	0.402	
Torso + head	0.498	0.531	0.506	0.503
Upper arm	0.356	0.336	0.348	0.322
Forearm	0.296	0.295	0.290	0.303
Forearm + hand	0.438	0.427	0.415	0.468
Upper extremity	0.384	0.372	0.363	0.368
Thigh	0.275	0.234	0.240	0.323
Lower leg	0.287	0.287	0.287	0.302
Lower leg + foot	0.384	0.380	0.383	0.416
Lower extremity	0.311	0.291	0.288	0.326

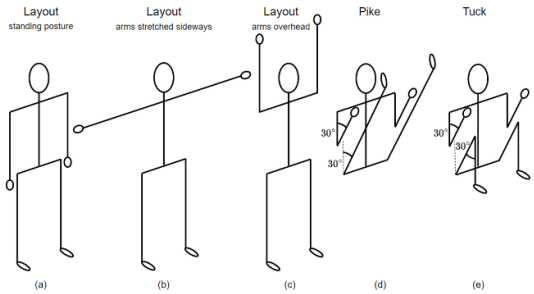

Figure 12. Five body postures relevant for competitive diving.

Table 3. Estimated moments of inertia ($kg \cdot m^2$) of the whole body about the transverse axis through the centre of gravity in the five postures shown in figure 12 for the two athletes and the 'average athlete' of Miller and Morrison [30].

Posture	Athlete 1	Athlete 2	Miller & Morrison
Layout (a)	11.3	14.0	14.5
Layout (b)	12.0	15.1	15.7
Layout (c)	14.3	18.5	18.9
Piked (d)	4.3	5.9	5.8
Tucked (e)	3.4	4.1	4.1

Another interesting aspect is the contribution of each segment to the total moment of inertia, considering local and remote terms. Applying Woolley's model [16] to the'average athlete' of Miller and Morrison [30], key insights show that local segmental moments of inertia are significant in computing the total moment of inertia and that the torso+head and lower extremities together contribute 90%–95% of the total moment of inertia in all postures, except when the arms are

Table 4. Contribution of each term (in percentage) to the total moment of inertia about the transverse axis through the centre of gravity for the 'average athlete' of Miller & Morrison [30].

Term	Layout (a)	Layout (b)	Layout (c)	Pike (d)	Tuck (e)
Local	22.8	20.5	17.5	57.3	80.3
Remote	77.2	79.5	82.5	42.7	19.7

overhead. This suggests that the upper extremities can be ignored when estimating the total moment of inertia in a piked posture, simplifying calculations. The estimated moment of inertia of the 'average athlete' in piked posture is 5.6 $\mathrm{kg \cdot m^2}$, barely different from 5.8 $\mathrm{kg \cdot m^2}$ when including the arms. The local and remote terms of the total moment of inertia are defined as the sums of the local and remote segmental moments, respectively. Table 4 shows the contributions of these terms for each posture in figure 12. In piked or tucked postures, the local term is more significant compared to the layout posture, as the extremities are closer to the body's CG in these postures.

5. Motion analysis of a 105B dive

Analysing somersaults in diving through video measurement is more complex than it seems. Mikl [8], Sayyah [33], and Sotheran [34] detail their data collection and analysis methods, using equipment from high-speed cameras to low-cost options, with frame rates of 120–250 fps. They discuss challenges like camera positioning, lighting, environmental conditions, camera calibration, and marker selection. Despite these challenges, students can still collect usable kinematic data. The main difficulty is in automatic tracking of markers, which often requires manual corrections due to interference and occlusion. But manual digitisation is possible, despite its time-consuming nature.

In this section, we present a motion analysis of a 105B dive carried out by Athlete 1 and recorded at frame rate of 100 fps. In this analysis, we assume that the athlete's arms and legs are straightened and move parallel after take-off, maintaining left-right symmetry. This reduces the model to three rigid bodies: torso+head, a pair of lower extremities, and a pair of upper extremities. Thus, we only need to collect position data for four key points: ankle, hip, shoulder, and wrist joint, each marked with kinesiology tape. While the upper extremities' movement is not entirely in the two-dimensional plane (e.g. forearms wrap around the legs in a piked posture), we use the shoulder and visible part of the arms as key points, justified by the minimal contribution of upper extremities to the total moment of inertia in a piked posture. After collecting data, we check the horizontal and vertical coordinates of each key point for errors, and apply noise reduction to the data via a cubic spline-smoothing algorithm [21] to improve results.

5.1. Estimation of the CG, somersault angle, and angular velocity

A key step in video analysis is calculating the athlete's CG during flight, along with the somersault angle α, and the angular velocity ω (the time-derivative of α). Figure 13 shows a snapshot of this analysis, covering a 105B dive from take-off to water entry. To the right of the video window, graphs of the x- and z-coordinates of CG are displayed. A linear fit of the x-coordinate indicates that CG moves horizontally at a constant speed of 1.11 $\mathrm{m\ s^{-1}}$. A parabolic fit of the z-coordinate shows a vertical initial speed v_z of 6.27 $\mathrm{m\ s^{-1}}$. The flight height h_{flight}, defined as the difference between the maximum height of CG and the height of CG at take-off, can be computed as $h_{\mathrm{flight}} = {v_z}^2/(2g)$. Using for the acceleration of gravity g the value it would have according to the parabolic curve fit, i.e. $g = 10.88\ \mathrm{ms^{-2}}$, we get a flight height of 1.81 m. The springboard significantly boosts this height compared to a standing jump. The built-in ruler in the video window measures the same value and therefore it can be used to determine the dive height h_{dive}, defined as the difference between the maximum height of CG and the height of CG at water entry: $h_{\mathrm{dive}} = 5.27$ m.

Flight time t_{flight}, defined as the time from the last instant of take-off, when the feet leave the springboard, until the athlete enters the water, can be calculated using

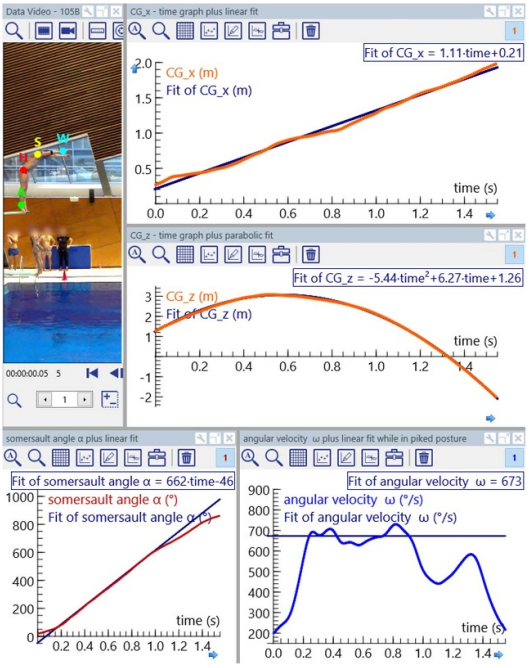

Figure 13. Screenshot of a video analysis in which the time course of CG, the somersault angle, and the angular velocity of Athlete 1 is estimated while he is airborne in a 105B dive.

$$t_{\text{flight}} = \frac{v_z + \sqrt{{v_z}^2 + 2g\,(h_{\text{CG,take-off}} - h_{\text{CG,entry}})}}{g},$$

where $h_{\text{CG,take-off}} - h_{\text{CG,entry}}$ is the height difference of CG at the last instant of take-off and at the first instant of water entry, respectively. This results in a flight time of 1.54 s, a value that can also be read off from the graph in scanning mode by scrubbing the video, i.e. by advancing or reversing a video clip manually for the purpose of precisely identifying and marking interesting events in the movie and to relate them with graphical features (e.g. coordinates of key variables).

The somersault angle α is computed using the slope of the line through the centres of gravity of the lower extremities and the torso + head segment, with step functions added to ensure continuity. The graph of α (figure 13, lower-left) is nearly linear during the piked posture, with a constant angular velocity ω of 662 °/s from linear regression. The start and end of the dive show lower angular velocities. The graph of the angular velocity (figure 13, lower-right), computed using a spline smoothing algorithm [21], shows a similar value of 673 °/s.

These calculations and measurements show students that multiple methods can estimate kinematic variables, enhancing accuracy and reliability in analyses, and that contextual graphs provide valuable insights into visible video events.

5.2. Angular velocities of body segments

For deeper understanding of body motion during a 105B dive, analysing the angular velocities of body segments is essential. Figure 14 presents annotated graphs of the computed angular velocities for the arms, torso + head, and legs. The graphs show that the arms rotate quickly downward at the dive's beginning, a motion that starts during the last phase of take-off while the athlete is still in contact with the springboard, and then slows down. The torso+head segment also rotates fairly rapidly, with its angular velocity increasing as the athlete transitions to a piked posture. Initially, the lower extremities rotate slower than other segments but soon catch up, with all segments reaching and fluctuating around a constant angular speed of 673 °/s. This indicates that in a piked posture, the athlete's segments move together, and their angular velocities align with the total body's angular velocity, estimated as the rotation of the chosen line of body orientation. As the athlete prepares for water entry, the graphs reveal that the rotation speed of the arms and torso+head segment decreases first, followed by a reduction in the legs' rotation speed. The athlete begins opening the piked posture by removing his hands from his legs and abducting his arms to the side when his legs are at 10 o'clock position. He maintains the piked posture, reaching a local minimum of angular velocity with his legs at 2 o'clock position. Interestingly, in this dive, after the deceleration due to opening the piked posture, there is a temporary increase in angular velocity as the athlete prepares for water entry. Walker [35, figure 9] observed a similar pattern, suggesting it might be 'due to the shoulders adducting after initial abduction, resulting in a reduction in the mass moment of inertia, in preparation of the straight arm line for water entry.' However, in our video, we notice that the athlete temporarily bends his hips more strongly, from a hip shape angle of 89°

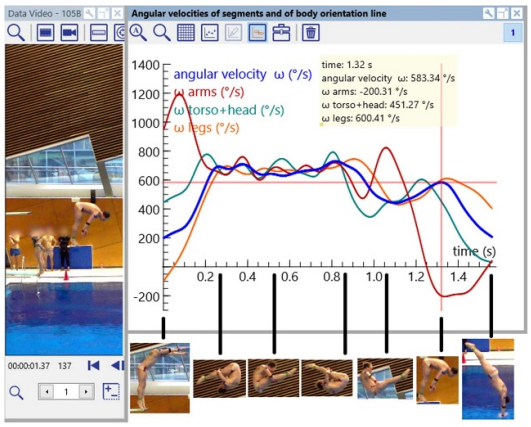

Figure 14. Screenshot of a video analysis showing the time courses of the angular velocities of segments and the total body during a 105B dive. The screenshot is annotated with images of body postures at key events during flight. The video captures the athlete preparing for entering the water.

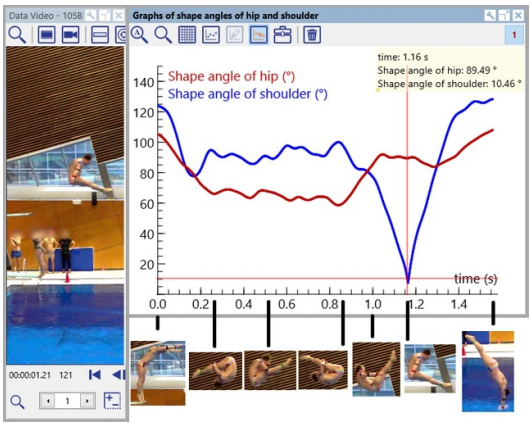

Figure 15. Screenshot of a video analysis showing the time courses of the hip and shoulder shape angles during a 105B dive. The picture is annotated with images of body postures at key moments during flight. The video captures the athlete's piked posture with his arms close to the body.

at 3 o'clock position of his legs to 82° at 6.30 o'clock position of his legs (as shown in figure 14 at times 1.06 s and 1.32 s, respectively), reducing the moment of inertia and thus increasing angular velocity.

When students do a similar motion analysis of a somersault and analyse angular velocity graphs, they may experience that it makes sense to divide the dive flight into differing phases, and that graphs provide detailed information about segmental body motions in a real diving context, which might be challenging to discern directly from a video clip.

5.3. *The shape angles of hip and shoulder*

Key kinematic variables for the 105B dive are the shoulder-hip-ankle angle and the wrist-shoulder-hip angle, also known as the hip and shoulder shape angles, respectively. These angles are calculated using the cosine rule. For example, the hip shape angle is given by

$$\text{hip shape angle} = \arccos\left(\frac{{d_{\text{HA}}}^2 + {d_{\text{HS}}}^2 - {d_{\text{AS}}}^2}{2 d_{\text{HA}} d_{\text{HS}}}\right),$$

where d_{HA} is the distance between hip and ankle joint, d_{HS} is the distance between hip and shoulder joint, and d_{AS} is the distance between ankle and shoulder joint. This formula underscores the importance of mathematics in physics studies.

Figure 15 shows annotated shape angle graphs. The extra bending of the hips while the athlete prepares for water entry is visible as a little dip in the graph of the hip shape angle near the end of the flight phase. But what really catches the eye is the 'spike' in the graph of the shoulder shape angle, due to rapid motion of the arms downward, followed by a rapid motion to get them overhead. The objective for having the arms close to the body for a brief moment during flight could be to aesthetically please the judges by clearly showing the pike posture. However, a better reason for using this so-called pike-out come-out technique [36, 37] is that it allows more time to see the entry point and more opportunity to adjust the water entry, when the body is straightened and the arms are brought overhead. When there is not a lot of time to prepare for water entry, the straight-line come-out technique is mostly used.

5.4. *Moments of inertia of segments and the total body*

Moments of inertia of segments and the total body can be estimated using the formulas of Woolley's model of the human body [16]; see section 4 and the supplementary file *Anthropometric model of*

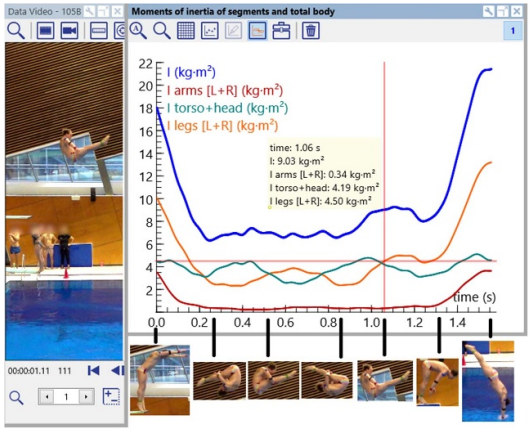

Figure 16. Screenshot of a video analysis showing graphs of the moments of inertia of segments and total body during a 105B dive. The picture is annotated with images of body postures at key moments during flight. The video captures the athlete's piked posture just after opening his deepest pike.

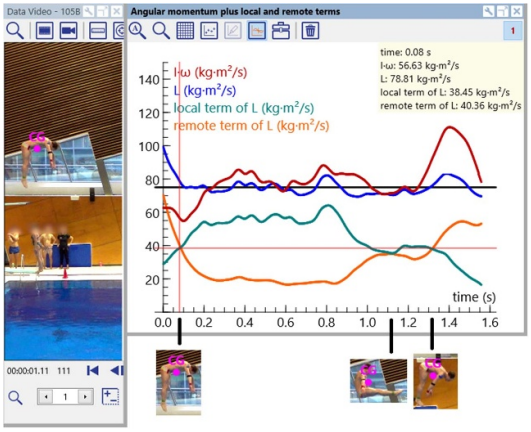

Figure 17. Graphs of the total angular momentum L while the athlete is airborne in a 105B dive, estimated by two methods: $L = I \cdot \omega$ (red curve) and $L = L_{\text{local}} + L_{\text{remote}}$ (blue curve), where $L_{\text{local}} = \sum_s I_s \cdot \omega_s$ and $L_{\text{remote}} = \sum_s m_s \cdot \left[\vec{r_s} \times \vec{v_s} \right]_3$. The horizontal black line indicates the best constant angular momentum L. The annotations show postures when the local and remote terms are equal.

man. Figure 16 shows graphs of these estimated moments of inertia while the athlete is airborne in the 105B dive. The moment of inertia of the arms is small compared to the legs and torso + head while the athlete is in a piked posture, where the moments of inertia of the legs and torso + head are similar. The graphs illustrate how the athlete reduces inertia in the piked posture, allowing faster rotation: in $\text{kg} \cdot \text{m}^2$, from 18.2 at take-off to 6.8 in the piked posture, to 21.4 in the layout with arms overhead. These values, though higher than those in table 3 for Athlete 1, align with values reported in research literature (e.g. [19], figures 6–34). The dip in the moment of inertia near the end when the athlete is preparing for water entry is visible. It is caused by a dip in the moment of inertia of both legs and the torso+head.

5.5. Angular momenta of segments and the total body

We aim to verify that the angular momentum of the athlete's body, obtained at take-off, remains constant while airborne. We explore methods for estimating the angular momenta of segments and the total body, distinguishing between local and remote components. In section 2.4, we discussed two methods for estimating angular momenta. The first method uses a line of body orientation and the formula $L = I \cdot \omega$, where I is the moment of inertia about the transverse axis through the body's CG and ω is the angular velocity of the somersault angle. This method is approximate and works only when the hip and shoulder shape angles do not change. The second method accounts for changing shape angles and includes a local and remote term.

Figure 17 shows the graph of the total angular momentum estimated by both methods. When the athlete is in the piked posture, both graphs can be approximated by a horizontal regression curve with a constant value of $75\ \text{kg} \cdot \text{m}^2\text{s}^{-1}$. The second method's graph aligns better throughout the flight, supporting the law of conservation of angular momentum. Figure 17 also highlights that both local and remote terms contribute significantly to the total angular momentum L, with the local term largest during the piked posture and smallest in layout postures at take-off and water entry, consistent with the results in table 4 for an 'average athlete'.

Figure 18 shows the graphs of the angular momenta of segments and total body while the

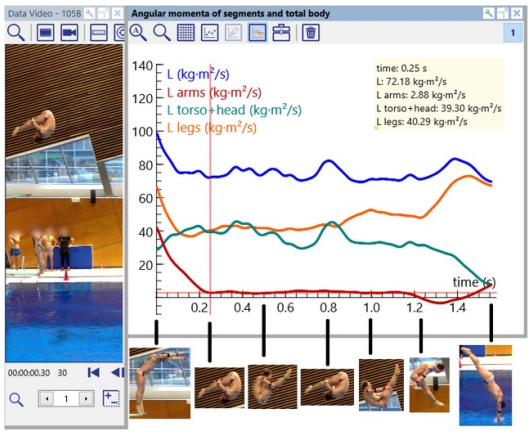

Figure 18. Graphs of angular momenta of segments and total body while the athlete is airborne in a 105B dive. The video captures the start of the piked posture of the athlete.

athlete is airborne during the 105B dive. At take-off, the arms have substantial angular momentum, as the athlete is still swinging his arms rapidly towards his torso. Once the athlete reaches the piked posture with a fixed shoulder angle, the arms' angular momentum becomes negligible. In this posture, the torso+head and legs contribute almost equally to the angular momentum, consistent with the earlier findings (figure 16) that these segments have similar moments of inertia.

5.6. Estimating various kinematic measures

Easier student activities include estimating and comparing kinematic measures such as dive height, total flight time, body orientation angle, hip and shoulder shape angles at take-off and water entry, and angular displacement during the dive. For these activities, it suffices to collect position data of some key points of the human and create graphs of the time course of kinematic variables. Scrubbing video clips and simultaneously observing key events in the graphs, recording the times when they occur, and using digital measurement tools like a ruler and protractor in the video analysis environment is all what is needed. The required mathematical skills in such activities are kept at upper-secondary level when one uses an easily marked line of body orientation for the somersault angle, for instance, the line through the knee and the shoulder. These activities let students think about how to define the kinematics variables and how to measure or estimate them, which is an opportunity for discussion and broadened understanding.

Table 5. Measured quantities for a 105B and 107B dive.

Measure	105B	107B
Take-off body alignment (°)	23	43
Take-off hip angle (°)	141	123
Take-off shoulder angle (°)	139	120
Entry body alignment (°)	148	136
Entry hip angle (°)	168	140
Entry shoulder angle (°)	153	147
Total flight duration (s)	1.54	1.50
Total flight angular displacement (°)	845	1173

5.7. Comparing dive types

Estimating and comparing kinematic measures of differing dive types, and trying to understand similarities and differences in results adds to the understanding of the biomechanics of springboard diving. In the supplementary *Long write-up* we present a motion analysis of a 107B dive similar to the 105B dive analysis in this paper. Here, we mention main differences.

Table 5 compares kinematic measures for the 105B and 107B dives. In a 107B dive, the athlete leans more forward at take-off (larger take-off body alignment) by bending more his hips (smaller take-off hip angle). This leads to a lower dive height and consequently to a shorter total flight. The arms are thrown more rapidly downwards at take-off (smaller take-off shoulder angle). At water entry, the body is less straightened (smaller entry hip and shoulder angle) and vertically oriented (smaller entry body alignment). The athlete has not enough time to complete the $3\frac{1}{2}$ somersault: He misses angular displacement for a good water entry (smaller entry body alignment). The total flight angular displacement is always less than the specified angular displacement because of leaning at take-off, but in the 107B dive 87° is missing (compared to 55° in the 105B dive).

6. Conclusion

This paper explores opportunities for upper-secondary students and beyond to engage with rotational kinetics through somersaults. It highlights the ICT-supported interaction between the world of phenomena, in which empirical data is collected and analysed, and the world of theories, in which ideas are scientifically developed and further explored (see [38, 39]). In this case, the world of phenomena involves springboard diving and video measurements using COACH [5, 6]. The world of theories consists of angular kinematics, angular kinetics, and mathematical modelling of the human body. The student investigations presented aim to deepen understanding of concepts like moment of inertia and angular momentum by connecting them to real somersaults. Students learn to estimate moments of inertia using advanced mathematical models of the human body. We adhere to the advice of Laws and Pfizer [12]: 'We recommend that this type of angular momentum conservation project be undertaken only by capable, highly motivated students.' This certainly holds for the activities of using mathematical models to estimate moments of inertia and angular momenta. Students will need advice and guidance from their teachers. We hope that physics teachers are supported by the information provided in this paper and its supplementary files.

Data availability statement

All data that support the findings of this study are included within the article (and any supplementary files).

ORCID iD

André Heck https://orcid.org/0000-0002-7923-6360

Received 21 October 2024, in final form 2 December 2024
Accepted for publication 16 December 2024
https://doi.org/10.1088/1361-6552/ad9fcb

References

[1] Townend S 1993 Modelling the gymnastics giant swing—is it potentially dangerous? *Tech. Math. Appl.* **12** 163–5

[2] Heck A, Knobbe D, Nijdam N, Slooten O and Uylings P 2011 Exploring the giant circle on the high bar with ICT tools *Enhancing Mathematics Education Through Technology (Proc. ICTMT10)* ed M Joubert, A Clark-Wilson and M McCabe (University of Portsmouth) pp 134–40

[3] Contakos J, Carlton L, Thompson B and Suddaby R 2009 The physics of a gymnastics flight element *Phys. Teach.* **47** 355–61

[4] Page R 1976 The mechanics of swimming and diving *Phys. Teach.* **14** 72–80

[5] Heck A, Kedzierska E and Ellermeijer T 2009 Design and implementation of an integrated computer working environment *J. Comput. Math. Sci. Teach.* **28** 147–61

[6] Heck A 2012 Perspectives on an integrated computer learning environment *Doctoral Thesis* University of Amsterdam (available at: https://dare.uva.nl/record/409820)

[7] FINA Technical Diving Committee 2020 FINA diving officials manual (available at: www.fina.org)

[8] Mikl J 2015 All spun out *PhD thesis* University of Sidney (available at https://hdl.handle.net/2123/15375)

[9] Yeadon M 1984 The mechanics of twisting somersaults *Doctoral Thesis* University of Loughborough (available at https://hdl.handle.net/2134/7502)

[10] Close H and Heron P 2011 Student understanding of the angular momentum of classical particles *Am. J. Phys.* **79** 1068–78

[11] Mashood K 2014 Development and evaluation of a concept inventory in rotational kinematics. *PhD Thesis* (available at: https://hdl.handle.net/10603/406312)

[12] Laws P and Pfister H 1998 Using digital video analysis in introductory mechanics projects *Phys. Teach.* **36** 282–7

[13] Williamson J, Torres-Isea R and Kletzing C 2000 Analyzing linear and angular momentum conservation in digital videos of puck collisions *Am. J. Phys.* **68** 841–7

[14] Heck A and Uylings P 2005 Yoyo Joy *Visions of Mathematics Education: Embedding Technology in Learning (Proc. ICTMT7)* vol 2, ed F Olivero and R Sutherland (University of Bristol) pp 237–44

[15] Fäldt Å and Fredlund T 2023 The gyroscopic effect and moment of inertia *Phys. Educ.* **58** 025001

[16] Woolley C 1972 Appendix A: segment masses, centers of mass, local moments of inertia for an anthropometric model of man B A Conway *Development of Skylab Experiment T-013 Crew/Vehicle Disturbances (NASA TN-6584)* (NASA

Langley Research Center) (available at: https://ntrs.nasa.gov/api/citations/19720007227/downloads/19720007227.pdf)
[17] Zeni J, Thomas S and Winter D 2023 *Winter's Biomechanics and Motor Control of Human Movement* 5th edn (Wiley)
[18] Robertson G, Caldwell G, Hamill J, Kamen G and Whittlesey S 2014 *Research Methods in Biomechanics* 2nd edn (Human Kinetics)
[19] Hay G 1993 *The Biomechanics of Sports Techniques* 4th edn (Prentice Hall)
[20] Foss S 1969 A method for obtaining initial estimates of the parameters in exponential curve fitting *Biometrics* **25** 580–4
[21] Ramsay J and Silverman B 2005 *Functional Data Analysis* (Springer) pp 179–81
[22] Frohlich C 1979 Do springboard divers violate angular momentum conservation *Am. J. Phys.* **47** 583–92
[23] Edwards M 1986 Zero angular momentum turns *Am. J. Phys.* **54** 846–7
[24] Essén H and Nordmark A 2018 A simple model for the falling cat problem *Eur. J. Phys.* **39** 035004
[25] Knudson D 2013 *Qualitative Diagnosis of Human Movement: Improving Performance in Sport and Exercise* 3rd edn (Human Kinetics)
[26] Barter J 1957 *Estimation of the Mass of Body Segments (WADC TR 57–260)* (Wright-Patterson Air Force Base)
[27] Clauser C, McConville J and Young J 1969 *Weight, Volume, and Center of Mass of Segments of the Human Body* AMRL TR 69–70 Wright-Patterson Air Force Base, OH (available at: https://apps.dtic.mil/sti/tr/pdf/AD0710622.pdf)
[28] Hanavan E 1964 *A Mathematical Model of the Human Body (AMRL TR 64–102)* (Wright-Patterson Air Force Base) available at: https://apps.dtic.mil/sti/pdfs/AD0608463.pdf
[29] Project Jupyter (available at: https://jupyter.org)
[30] Miller D and Morrison W 1975 Prediction of segmental parameters using the Hanavan human body model *Med. Sci. Sports* **7** 207–12
[31] Dempster W 1955 *Space Requirements of the Seated Operator* WADC TR 55–169 Wright-Patterson Air Force Base, OH (available at: https://apps.dtic.mil/sti/citations/tr/AD0087892)
[32] Whittset C 1963 *Some Dynamic Response Characteristics of Weightless Man (AMRL TR 63–18)* (Wright-Patterson Air Force Base) (available at: https://apps.dtic.mil/sti/tr/pdf/AD0412451.pdf)
[33] Sayyah M 2017 Variability and control in springboard diving *PhD Thesis* University of Loughborough (available at: https://hdl.handle.net/2134/33552)
[34] Sotheran A 2019 Real-time analysis and feedback of performance indicators in elite diving *PhD Thesis* Sheffield Hallam University (https://doi.org/10.7190/shu-thesis-00397)
[35] Walker C 2017 Functional analysis of stability and variability in multiple forward somersaulting dives from the 3m springboard *PhD Thesis* University of Sidney (available at https://hdl.handle.net/2123/17351)
[36] O'Brien R 2002 *Springboard and Platform Diving* 2nd edn (Human Kinetics)
[37] Huber J 2016 *Springboard and Platform Diving* (Human Kinetics)
[38] Millar R, Tiberghien A and Le Maréchal J-F 2002 Varieties of labwork: a way of profiling labwork tasks *Teaching and Learning in the Science Laboratory* ed D Psillos and H Niedderer (Kluwer Academic Publishers) pp 9–20
[39] Van den Berg E 2009 The PCK of teaching in the laboratory: turning manipulation of equipment into manipulation of ideas *Teachers' Professional Knowledge in Science and Mathematics Education: Views from Malaysia and Abroad* ed O de Jong and L Halim (Faculty of Education, Universiti Kebangsaan) pp 85–110 (available at: www.iederkindeentalent.nl/wp-content/uploads/2012/06/The-PCK.pdf)

André Heck earned MSc degrees in mathematics and chemistry, and a doctoral degree in mathematics and science education. He is senior lecturer at the Faculty of Science of the University of Amsterdam. His research area is the application of ICT in mathematics and science.

Sebastian van Baarsen is currently the best Dutch high diver and a former Dutch champion in springboard diving. He is physical education teacher at Fons Vitae Lyceum in Amsterdam, dyslectic, and manager of Indoor Cliff Diving.

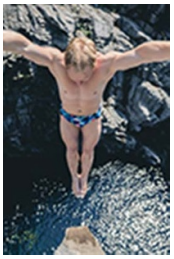

Jan Wilko Heinzel (33) is one of the best 20m high divers and has won multiple international titles around the world. Next to his breathtaking passion he is a studied meteorologist working at a big IT company in Amsterdam. He is also a board member of Infinite Drop, an international high diving association based in Switzerland.

Ad Mooldijk earned his MSc degree in physics. He was teacher in secondary education and teacher trainer at Utrecht University. After retirement, he is now educational employee at CMA-Science in Amsterdam and coordinates the National Physics Olympiad.

Norbert van Veen is a secondary school physics teacher and part-time physics education employee of CMA-Science.